



Petrography, microthermometry, and isotopy of the gold veins from Vetás, Santander (Colombia)

Sonia Rojas Barbosa¹, Juan Carlos Molano Mendoza², Thomas Cramer²

¹Servicio Geológico Colombiano

²Universidad Nacional de Colombia

* Corresponding author: srojasb@unal.edu.co; jcmolanom@unal.edu.co

ABSTRACT

The gold mineralization located in Vetás, Santander, consists of auriferous quartz veins hosted in Bucaramanga gneiss rocks, intrusive Jurassic rocks, and intrusive to porphyritic Miocene rocks. This study identified four mineralizing events: (1). Sericite, carbonate (ankerite and calcite?), massive and microcrystalline quartz, sphalerite, adularia, albite, galena, thin pyrite, pyrrhotite, chalcocopyrite. The age for this stage is 10.78 ± 0.23 Ma (Ar/Ar on sericite). (2). Molybdenite, magnetite with exsolution of ilmenite, As-pyrite, sphalerite, fine-grained pyrite and little chalcocopyrite quartz with huge, feathery, fine mosaic, flamboyant and microcrystalline textures and, tourmaline and sericite. (3). Gold and tennantite associated with sphalerite, fine- and coarse-grained pyrite, As-pyrite, chalcocopyrite like inclusions, and quartz with flamboyant, mosaic, massive and "comb" textures, and tourmaline. Stage 2 and 3 happened from 7.58 ± 0.15 Ma to 6.89 ± 0.41 Ma (Ar/Ar on sericite). (4). Thick, thin, and pyrite with arsenic, hematite and microcrystalline quartz (forming breccia texture), and sericite. The age for this stage is 5.24 ± 0.10 (Ar/Ar on sericite). Post-mineral: quartz comb, alunite, halloysite, kaolinite, and ferrum hydroxides.

The stable isotopes, $\delta^{18}\text{O}$, δD , and $\delta^{34}\text{S}$ and fluid inclusions analysis infer that fluids were producing a mixture of meteoric and magmatic fluids with low salinity and minimum trapping temperatures between 200°C to 390°C .

The mineralogy association, and fluid inclusions, in the first event show characteristic of low sulfidation epithermal. The second stage was hottest and with more magmatic signature overprinted an intermediate sulfidation system; show a little more salinity on the fluids and more mineralogical diversity, the third and four events, could show an evolution of this fluid, where it was cooling and impoverishing on metals. Two initial stages are contemporaneous with two magmatic Miocene pulses on the area: the first one of granodiorite composition 10.9 ± 0.2 Ma (U/Pb zircon), and the other one rhyodacite with 8.4 ± 0.2 y 9.0 ± 0.2 Ma.

Keywords: stable isotopes; epithermal; intermediate sulfidation; gold mineralization; fluids mixture; Miocene.

Petrografía, microtermometría e isotopía de las vetas auríferas de Vetás, Santander (Colombia)

RESUMEN

La mineralización de oro ubicada en Vetás, Santander, consiste en vetas auríferas de cuarzo alojadas en rocas del gneis de Bucaramanga, rocas jurásicas intrusivas y rocas intrusivas porfiríticas miocénicas. Este estudio identificó cuatro eventos de mineralización: (1). Sericita, carbonato (ankerita y calcita?), cuarzo masivo y microcristalino, esfalerita, adularia, albita, galena, pirita delgada, pirrotita, calcopirita. La edad para esta etapa es 10.78 ± 0.23 Ma (Ar / Ar en sericita). (2). Molibdenita, magnetita con exsolución de ilmenita, arsenopirita, esfalerita, pirita de grano fino un poco de calcopirita y cuarzo con textura plumosa, mosaico fino, flamboyante y microcristalino, turmalina y sericita. (3). Oro y tenantita asociados con esfalerita, pirita de grano fino y grueso, pirita de arsenopirita, calcopirita como inclusiones, y cuarzo con texturas flamboyante, mosaico, masiva y en "peine", y turmalina. Los eventos 2 y 3 ocurrieron entre los 7.58 ± 0.15 Ma a 6.89 ± 0.41 Ma (Ar / Ar en sericita). (4). Pirita en cristales finos y gruesos con arsénico, hematita y cuarzo microcristalino (formando una textura brechosa), y sericita. La edad para este evento es de 5.24 ± 0.10 (Ar / Ar en sericita). El evento Post-mineral: peine de cuarzo, alunita, halosita, caolinita e hidróxidos de hierro.

Los isótopos estables, $\delta^{18}\text{O}$, δD y $\delta^{34}\text{S}$ y el análisis de inclusiones de fluidos infieren que los fluidos fueron producto de una mezcla de fluidos meteóricos y magmáticos con baja salinidad y temperaturas de atrapamiento mínimas entre 200°C y 390°C . La asociación mineralógica y las inclusiones fluidas, en el primer evento, muestran características de un ambiente epitermal de baja sulfuración; el segundo evento más caliente presenta una firma magmática más prominente sobreimponiendo un sistema epitermal de intermedia sulfuración sobre el de baja sulfuración, con un poco más de salinidad en los fluidos y más diversidad mineralógica. Para el tercer y cuarto eventos muestran una evolución de este fluido, donde se enfría y se empobrece en metales. De acuerdo a las edades reportadas, los dos eventos iniciales son contemporáneos con dos pulsos magmáticos del Mioceno que fueron identificados en sectores circundantes del área, el primero de composición de granodiorita 10.9 ± 0.2 Ma (citrón U / Pb, Mantilla, et al. 2011), y el otro de riodoritas con 8.4 ± 0.2 y 9.0 ± 0.2 Ma.

Palabras clave: Isotopos estables, epitermal, sulfuración intermedia, mineralización aurífera, mezcla de fluidos, Mioceno.

Record

Manuscript received: 22/03/2018

Accepted for publication: 24/04/2019

How to cite item

Rojas Barbosa, S., Molano Mendoza, J. C., & Cramer, T. (2020). Petrography, microthermometry, and isotopy of the gold veins from Vetás, Santander (Colombia). *Earth Sciences Research Journal*, 24(1), 5-18. DOI: <https://doi.org/10.15446/esrj.v24n1.63443>

Introduction

This work shows the physicochemical characteristics of the mineralizing fluids, and determine the possible metallogenic environment in which it was formed in addition to its age, based on petrographic, fluid inclusions, and isotopic studies.

The Vetas gold deposit is located in the area of Vetas, Santander, 50 km far from Bucaramanga toward the NE. Tectonically, the area is placed at the northwest of South American plate, limited by the Bucaramanga fault (principal regional structure on the area) and the Oca Fault. Those faults are strike-slip types, and the movement is a product of the subduction of Nazca and Caribbean Plate (Figure 1). Mineralization is undertaken as a series of veins embedded in metamorphic rocks of Bucaramanga gneiss and Jurassic-Tertiary igneous rocks that intrude them.

Geological setting

The study area is located in Santander Massif, which consists of Precambrian, metamorphic rocks, Jurassic intrusive igneous rocks, and Tertiary subvolcanic rocks (Miocene), also with colluvial deposits (Figure 1).

Bucaramanga gneiss rocks

In this area are outcrops paragneisses (quartz-feldspathic, quartz-biotitic, quartz feldspathic, and biotitic and silimanitic), quartzites and amphibolites. These rocks present retrograde metamorphism for biotite, evidenced by the

presence of chlorite (Urueña & Zuluaga, 2011). These rocks have a strong hydrothermal alteration, as evidenced by the presence of chlorite, epidote, feldspar, sericite, carbonates, and silicification associated with plagioclase and aluminosilicates, and veins.

Jurassic intrusive igneous rocks

Petrographically, these rocks are holocrystalline, fine-to-medium grained with a very light pink and gray color; their composition varies from granite, diorite, and tonalitic igneous rocks, and correspond to different bodies but contemporaneous (Ward *et al.*, 1973); which lie in the north and east of the study area (Figure 1). These rocks, close to mineralization zone have a moderate and zoned hydrothermal alteration, characterized by silicification and pyritization on the periphery and argillic alteration near the mineralized veins. The argillic alteration is strong and pervasive masking of the rock's original texture. These rocks are strongly fractured, helping the formation of stockwork mineralization.

Miocene intrusive rocks

These rocks occur as intrusives and dikes outcropping in the northern part of the study area, in the road to Reina de Oro Mine and within a few tunnels. The rocks are porphyritic quartzmonzonites, light pinkish to gray and composed of quartz, plagioclase (oligoclase) and biotite, zircon as accessories.

In some tunnels some dikes of this unit were observed cutting veins. In the La Reina de Oro tunnel, a sample of dacite was taken, where fine disseminated pyrite, arsenious pyrite, chalcocopyrite and magnetite (Figure 2) was identified.

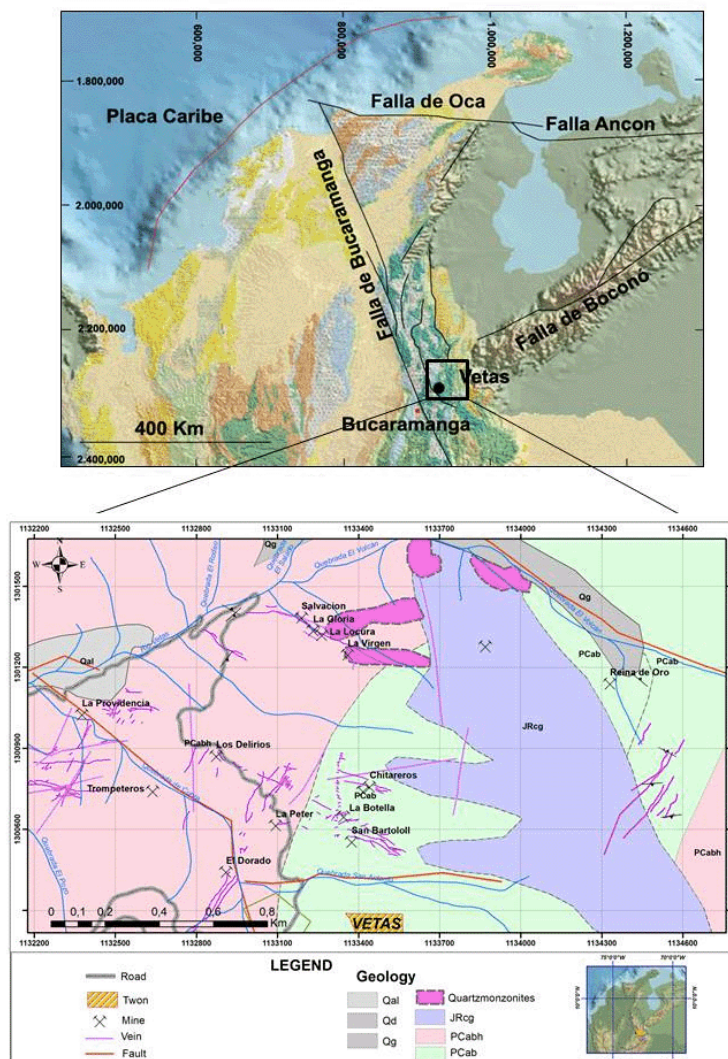


Figure 1. Location of the study area and tectonic setting (modified from Rojas, 2013; Ward *et al.*, 1973).

Structural Control setting

The Vetás mineralizations have a structural control related to the Bucaramanga (NW direction), Cucutilla (NE direction) faults, and their associated structures, which create a distensive tectonically originating spaces that served as conduits where the bodies were emplaced (Mantilla et al, 2009 and Mantilla et al, 2011).

Structurally reefs are related to fractures set with N55°W and N30°-60° strikes, with veins strikes of N30° to 50°E, N60° to 88°W and EW, and with dips between 30° to 90°. Dip variations are observed in places that vein thickness change (Mantilla and Mogollón, 1991), that situation is caused for little faults that cut the reefs.

The El Volcán Fault has a sinistral (left-lateral) movement, moving veins from 10 to 15 meters. Other smaller faults with a NE strike late to mineralization are significant because they cause truncations and wedge veins (Figure 2 and 3).

Ore deposit mineralogy

The mineralization occurs mainly in veins with thicknesses ranging from 30 cm to 1 meter. The most of the veins are banded, where the central strip correspond to recrystallized quartz and sulphides, occasionally tourmaline and sericite, this area contains higher gold concentrations. On both sides of these bands of quartz are presented primary and recrystallized quartz, and sulfides, also a significant increase in the intensity of sericite alteration. The most outer part of the vein corresponds to an argillic and mineralized zone, which is characterized for a bluish green color, and also presents significant gold concentrations.

Gangue Minerals

Quartz is the most abundant mineral, and was identified in all mineralizing stages (4 mineralizing stages and the post mineral event). Quartz occur with different textures (Dong et al., 1995) that were used as a guide for recognizing the paragenetic sequence. These textures are:

1. Quartz with massive texture (characterized by the presence of large, subhedrales to eudral). It was identified in early mineralizing stages (first, second and third stages).
2. Quartz with flamboyant and feathery texture on the second stage.
3. Quartz with mosaic texture (figure 4b), occurs as irregular, fine-grained to micro-crystalline and aggregate. In the late events of mineralization (second and third stages).
4. Cryptocrystalline quartz (figure 4b), latest event and acts as a cement in places where brecciated texture is presented (fourth event)
5. Quartz with “comb” texture (figure 4 a), appears as prismatic medium to coarse-grained crystals, this texture was formed on the third stage mineralization and a post-mineral event.



Figure 3. Vein wedged by faulting, La Peter mine



Figure 2. Argillic dacite dike cutting by some mineralized veinlets, and the same time the dike cut other veins too. Reina de Oro Mine

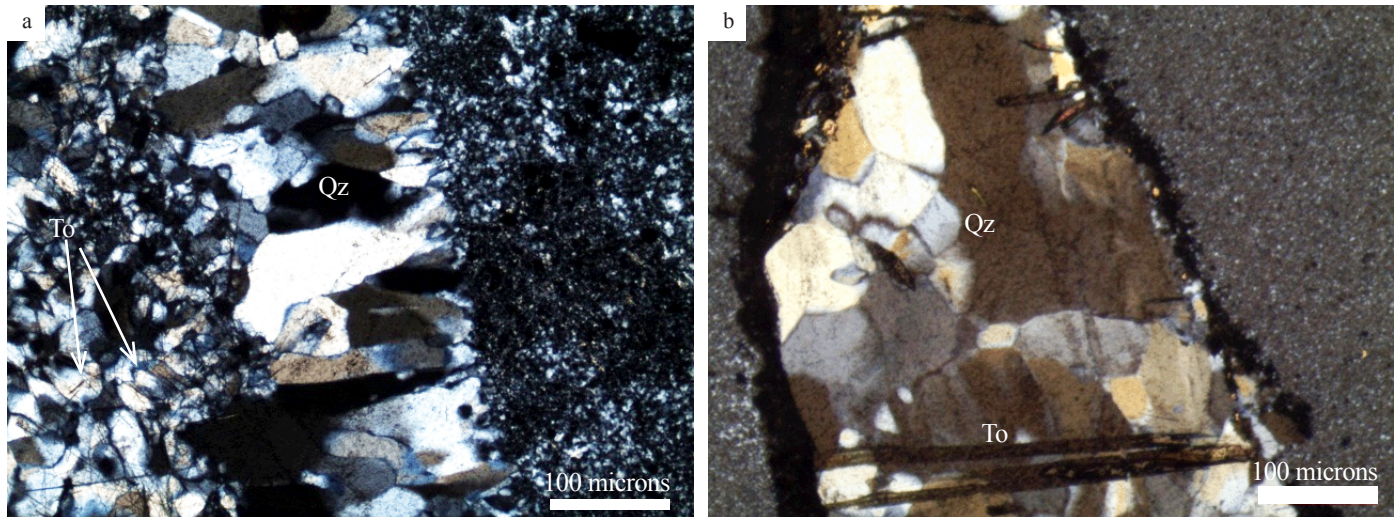


Figure 4. a. Quartz (Qz) textures. a. Quartz with “Comb” texture (center of the picture), Quartz with mosaic texture and tourmaline (left) of the third event, and microcrystalline quartz (right), b. Fragment of massive quartz with tourmaline (To) in a matrix of cryptocrystalline quartz (brecciated texture).

Ore Minerals

The paragenesis includes gold, sulfides like pyrrhotite, pyrite, tennantite, pyrrhotite, galena sphalerite and traces of molybdenite and oxides like, magnetite-ilmenite, the oxides being the most abundant. These minerals occur in veinlets or disseminated in intergrowth textures, replacement and filling spaces in the veins and host rocks.

Gold: It was identified in the third mineralizing stage, included in tennantite or fractures of low iron sphalerite (figure 5), and massive quartz associated with tourmaline and quartz with flamboyant and massive texture. Gold is irregularly shaped, its size varies between 26 and 41 μm . Other authors reported free gold associated with quartz and euhedral pyrite (Cortés, 2002 and Garcia y Uribe, 2003).

Silver: it has been reported in other works (Cortés 2002, Garcia y Uribe, 2003), and others) associated with pyrite and galena. Within the Electron probe micro-analyzer (EMPA) analysis show, between 10% and 15% Ag in the tennantite.

Pyrite: Three generations were identified: 1. Fine pyrite, 2. Coarse-grained (>100 microns) pyrite associated with As- pyrite (lighter and anisotropic) and 3. Fine-grained pyrite (± 50 microns, Figures 6 and 7). Some crystals of pyrite are product of recrystallization of pyrrhotite (Figure 6).

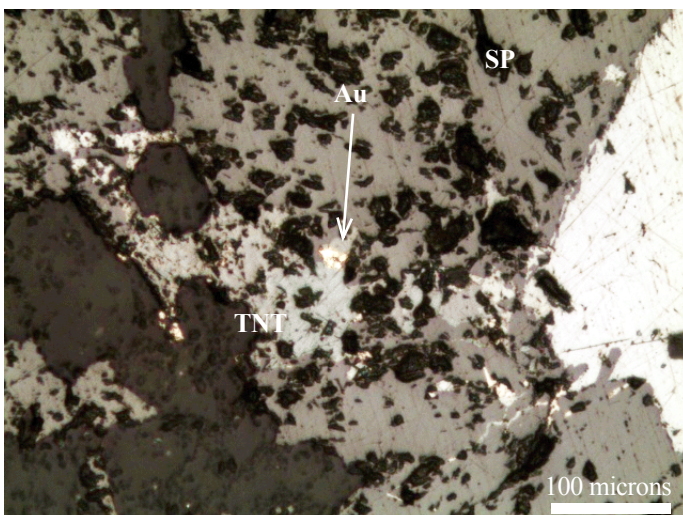


Figure 5. Gold (Au) include in tennantite (TNT), in paragenetic association with sphalerite and galena early.

Galena: It has coarse particle size (≥ 100 microns) and is associated with quartz with flamboyant and massive texture; in some cases, it is being replaced by sphalerite, so this indicates that was formed during first mineralizing event (figure 5 and 6).

Sphalerite: two species were identified, one clear and the other dark related to variations in the iron content possibly (Table 1). The first one crystallized during the first stage associated with carbonate when is disseminate in the host rock close to the veins and sericite, also appears as islands in pyrite, sometimes like inclusions and other times filling pores or associated with tennantite (Figure 5 and 6).

The clear (visible with transmitted light) sphalerite is found mainly in the central part of the veins, as coarse-grained, euhedral crystals. It can be found inter-grown with tennantite, replacing galena and pyrite and filling spaces in pyrite and As-pyrite.

Tennantite ($\text{Cu}_{12}\text{AgZn}_3\text{AsSb}_4\text{S}_{16}$ - $\text{Cu}_3\text{Ag}_2\text{ZnAsSb}_2\text{S}_8$): occurs in coarse-grained aggregate, with clear sphalerite. Its composition was determined by EMPA analysis (figure 5 and 6).

Molybdenite: is pinkish dirty pale gray color, with a fibrous and pseudo-hexagonal habit, presents a strong anisotropy and pleochroism. It occurs in the second stage of mineralization (Figure 6).

Chalcopyrite: occurs as pyrite islands in “atoll” textures or in contact (Figure 6) with fibrous crystal of molybdenite, indicating that they were precipitated on first to early second mineralization stages, even though some crystal of chalcopyrite occur in the three and four mineralizing event. According to some EMPA analysis, they contains arsenic in their composition (Figure 6).

Pyrrhotite: occurs as fine-grained, pink crystals, they are presented in the first mineralization event associated with chalcopyrite and dark sphalerite (Figure 6).

Magnetite: the magnetite have exsolutions of ilmenite, this indicate Ti in the structure of magnetite. This mineral appear in the second mineralization stage (Figure 6).

Alteration minerals and hydrothermal alterations

Sericite and illite (figure 7): main minerals alteration has good crystallinity and its size varies from fine to very coarse-grained (> 100 microns, possibly muscovite). It is presented as alteration in sillimanite and plagioclase alteration from the host rock, and is associated with sulfide and quartz veinlet in the first and second mineral stage, when the granulometry of sericite is fine-grained is presented with illite (identified by DRX).

Adularia: is the second alteration mineral in abundance, is found as coarse-grained (100 to 500 microns), euhedral crystals in veinlets, sometimes associated with albite and sericite. It represents in the first stage of mineralization.

Table 1. Sphalerite composition (EPMA Analysis)

Sample	As%	S%	Mn%	Fe%	Cu%	Zn%	Pb%	Ag%	Au%	Cd%	Sb%	Total%	Formule
1019	0,097	33,829	0,106	0,004	0,755	66,109	0,255	0,257	0,000	0,391	0,201	102,002	CuZnS
1019	0,161	33,376	0,112	0,000	0,580	66,170	0,209	0,401	0,015	0,482	0,301	101,806	CuZnS
1019	0,000	33,712	0,022	0,613	0,171	67,130	0,086	0,022	0,091	0,597	0,023	102,467	FeZnS
1019	0,000	34,001	0,042	0,977	0,233	66,600	0,106	0,015	0,000	0,398	0,013	102,384	FeZnS
1019	0,047	33,650	0,110	0,000	0,383	66,819	0,105	0,368	0,000	0,546	0,161	102,190	ZnS
1019	0,115	33,580	0,099	0,014	0,453	66,311	0,226	0,094	0,000	0,677	0,141	101,710	CdZnS
1019	0,094	33,551	0,073	0,000	0,288	66,771	0,091	0,181	0,000	0,498	0,149	101,695	ZnS
1019	0,000	33,761	0,106	0,000	0,166	67,069	0,099	0,067	0,000	0,498	0,017	101,781	ZnS
1019	0,439	32,604	0,123	0,000	1,148	64,029	0,248	0,968	0,083	0,461	0,397	100,500	CuZnS
1019	0,000	34,060	0,100	0,000	0,264	68,080	0,152	0,000	0,000	0,460	0,016	103,131	ZnS
1019	0,000	34,184	0,092	0,007	0,371	67,619	0,102	0,006	0,000	0,512	0,014	102,907	ZnS
1031	0,051	33,311	0,036	0,987	0,094	65,353	0,009	0,019	0,041	0,281	0,044	100,232	FeZnS
1031	0,000	33,228	0,039	2,199	0,201	65,827	0,056	0,000	0,021	0,248	0,000	101,818	Fe _{0,1} ZnS
1031	0,000	33,311	0,043	2,925	0,062	64,896	0,120	0,033	0,082	0,189	0,009	101,670	Fe _{0,1} ZnS
1031	0,000	33,190	0,000	1,051	0,001	67,632	0,134	0,020	0,000	0,348	0,000	102,375	ZnS
1031	0,000	33,276	0,039	1,992	0,150	66,101	0,175	0,028	0,000	0,232	0,044	102,038	Fe _{0,1} ZnS
1031	0,193	32,883	0,048	0,696	0,792	66,247	0,086	0,213	0,007	0,248	0,165	101,578	FeCuZnS
1035	0,000	32,994	0,073	0,649	0,208	66,544	0,018	0,028	0,131	0,260	0,107	101,011	FeZnS
1035	0,000	32,945	0,035	0,004	0,044	68,203	0,040	0,000	0,138	0,241	0,000	101,649	CuAgZnS
1035	0,000	33,196	0,008	0,007	0,025	68,747	0,095	0,000	0,297	0,245	0,002	102,622	ZnS
1035	0,000	32,905	0,014	0,000	0,130	68,493	0,231	0,033	0,090	0,213	0,000	102,109	ZnS
1035	0,000	32,818	0,028	0,016	0,257	67,990	0,000	0,128	0,000	0,340	0,049	101,657	ZnS
1035	0,046	33,095	0,070	0,008	0,384	67,346	0,134	0,293	0,000	0,272	0,135	101,783	ZnS
1035	0,010	32,756	0,037	0,572	0,153	67,342	0,102	0,217	0,097	0,290	0,088	101,672	ZnS
1035	0,077	32,997	0,035	0,026	0,386	67,484	0,105	0,138	0,000	0,364	0,174	101,783	ZnS
1035	0,000	32,978	0,049	0,020	0,055	68,332	0,201	0,035	0,103	0,284	0,000	102,057	ZnS
1035	0,072	32,817	0,056	0,016	0,524	67,130	0,173	0,340	0,041	0,328	0,236	101,732	ZnS
1035	0,025	33,067	0,023	0,233	0,212	67,703	0,156	0,128	0,000	0,278	0,119	101,943	ZnS
1035	0,000	42,300	0,076	0,028	0,319	67,880	0,153	0,039	0,341	0,000	0,000	111,174	ZnS
1019a	0,002	42,178	0,134	0,003	0,668	66,201	0,171	0,000	0,508	0,000	0,159	110,070	AuCuZnS

Ankerite (Identified by SEM) is restricted to the areas close to veins, where the rock alteration is not strong (figure 8).

Tourmaline: It is characterized by having prismatic habit, thin and elongated crystals with brownish green color. It is associated with the ore-rich

area of the veins, accompanied by quartz with flamboyant and massive texture between second and third stage.

Other identified alteration minerals include chlorite and epidote, in remote areas of the mineralization; kaolin, affecting feldspars from the host

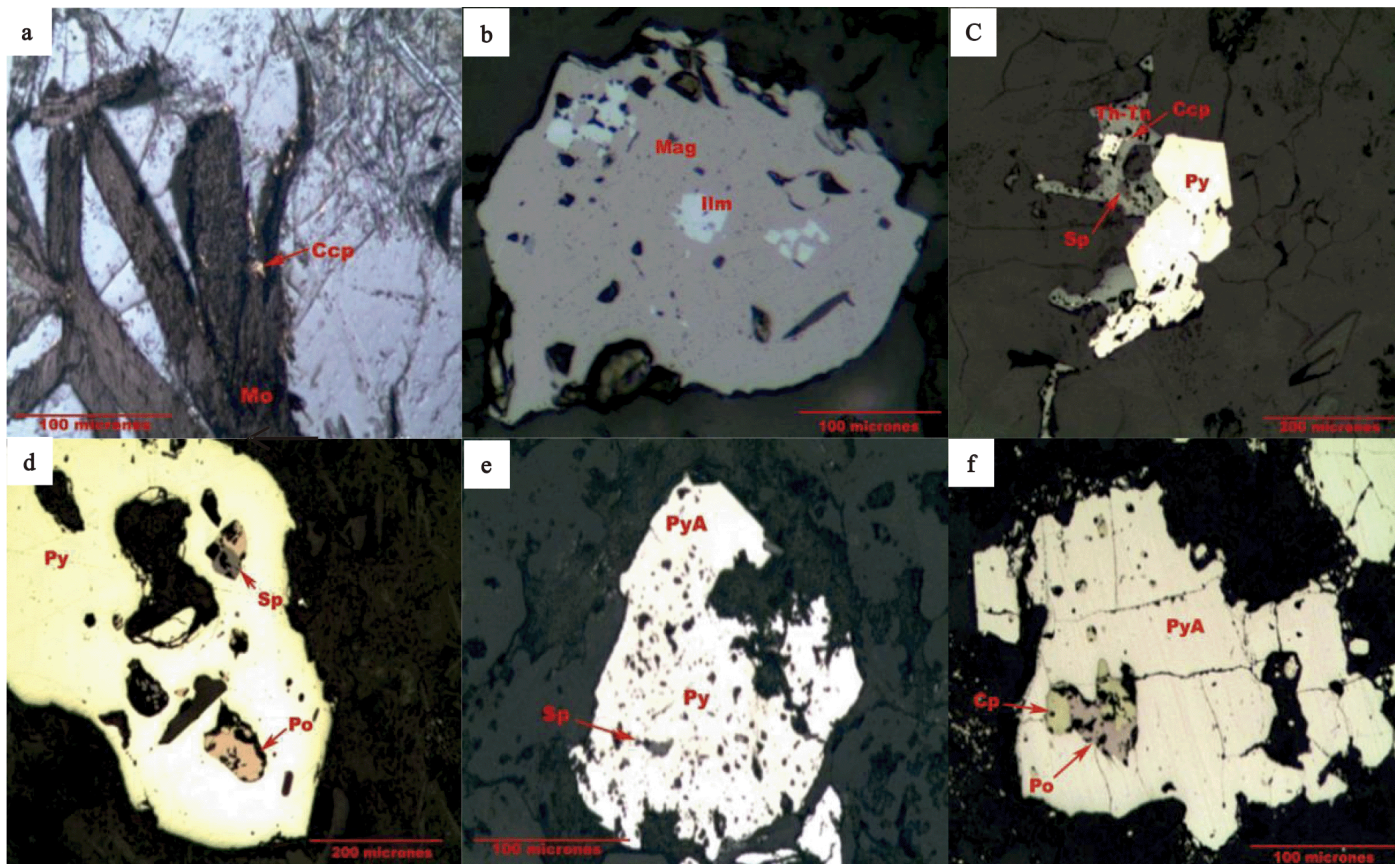


Figure 6. Ore minerals. a. Chalcopyrite crystals in the contact with molybdenite, b. Magnetite intergrowth with ilmenite exsolution, c. Tennantite in paragenesis with sphalerite and chalcopyrite, pyrite later or in paragenesis with sphalerite, d. Pyrrhotite and pyrite, before sphalerite, e. Ass-pyrite intergrown with pyrite (porous maybe product of pyrrhotite recrystallization) f. Chalcopyrite in paragenesis with pyrrhotite before As-pyrite.

rock and alunite (Identified by SEM and DRX), possibly product of supergene alteration as well as iron oxides and hydroxides are also recognized.

Paragenetic sequence

Four mineralizing events and one post-mineral stages separated by fracturing, brecciation and mineralogical changes were identified. Such associations are mentioned below and are represented in Figure 9:

Stage 1: association of sericite, carbonate (ankerite and calcite?), massive and microcrystalline quartz (possibly recrystallized Demoustier, Castroviejo, & Charlet, 1998), sphalerite, adularia, albite, galena, thin pyrite, pyrrhotite, chalcopyrite.

Mineralogical change is produced by a temperature increase and enrichment of fluids.

Stage 2: Molybdenite, magnetite with exsolution of ilmenite, As-pyrite, sphalerite, fine-grained pyrite and little chalcopyrite quartz with huge, feathery, fine mosaic, flamboyant (product of recrystallization of massive quartz first event or from chalcedony Demoustier, Castroviejo, & Charlet, (1998)) and microcrystalline textures quartz and, tourmaline and sericite.

Brittle deformation, which produced conduits where new minerals were mobilized and precipitated.

Stage 3: Gold and tennantite associated with sphalerite, fine-grained pyrite, coarse-grained pyrite and As-pyrite, sometimes with chalcopyrite like inclusions, and quartz with flamboyant, mosaic, massive and “comb” textures, and tourmaline.

Stage 4: Fine-grained pyrite microcrystalline quartz and sericite. A generation of fine-grained pyrite with microcrystalline quartz that produces brecciated textures.

Post-mineral stage: This event happens in open spaces result of brittle deformation or remaining space of crystallization, which where was formation of small quartz geodes with “comb” texture, ferrum hydroxide and alunite, halloysite and kaolinite.

Fluid inclusions microthermometry

The study of fluid inclusions provides information related to changes in the temperature and composition of the mineralizing fluids.

The measured fluid inclusions correspond to 1, 2, 3 mineralizing stage and the post-mineral event (Figure 10).

The research was carried out in five polished thin sections chosen because of their mineralogical characteristics and characterized by their textures and abundance of fluid inclusions that distinguish the different mineralizing pulses. The measured fluid inclusions correspond to 1, 2, 3 mineralizing events and the paragenetic post-mineral sequence (Figure 9). During the analysis, the following was discovered: biphasic inclusions (the most abundant), very small monophasic and three phasic (only two examples, with crystals of opaque minerals).

Biphasic inclusions have sizes ranging from less than 5 μm (the most abundant), 10 μm – 30 μm and the biggest range from 80 μm to over 100 μm . A lot of varieties of shapes are observed: Regular, irregular, ovoid and tabular. The primary inclusions in quartz with massive texture are the biggest, usually they appear lonely or as isolated groups and in the center of the crystals. Some pseudo-secondary inclusions are found as smaller aligned sets along microfractures that do not touch the edges of the crystals

Secondary inclusions were observed in the recrystallized edges of the quartz with flamboyant and feathery textures or in fractures that cross a lot of crystals (Figure 11).

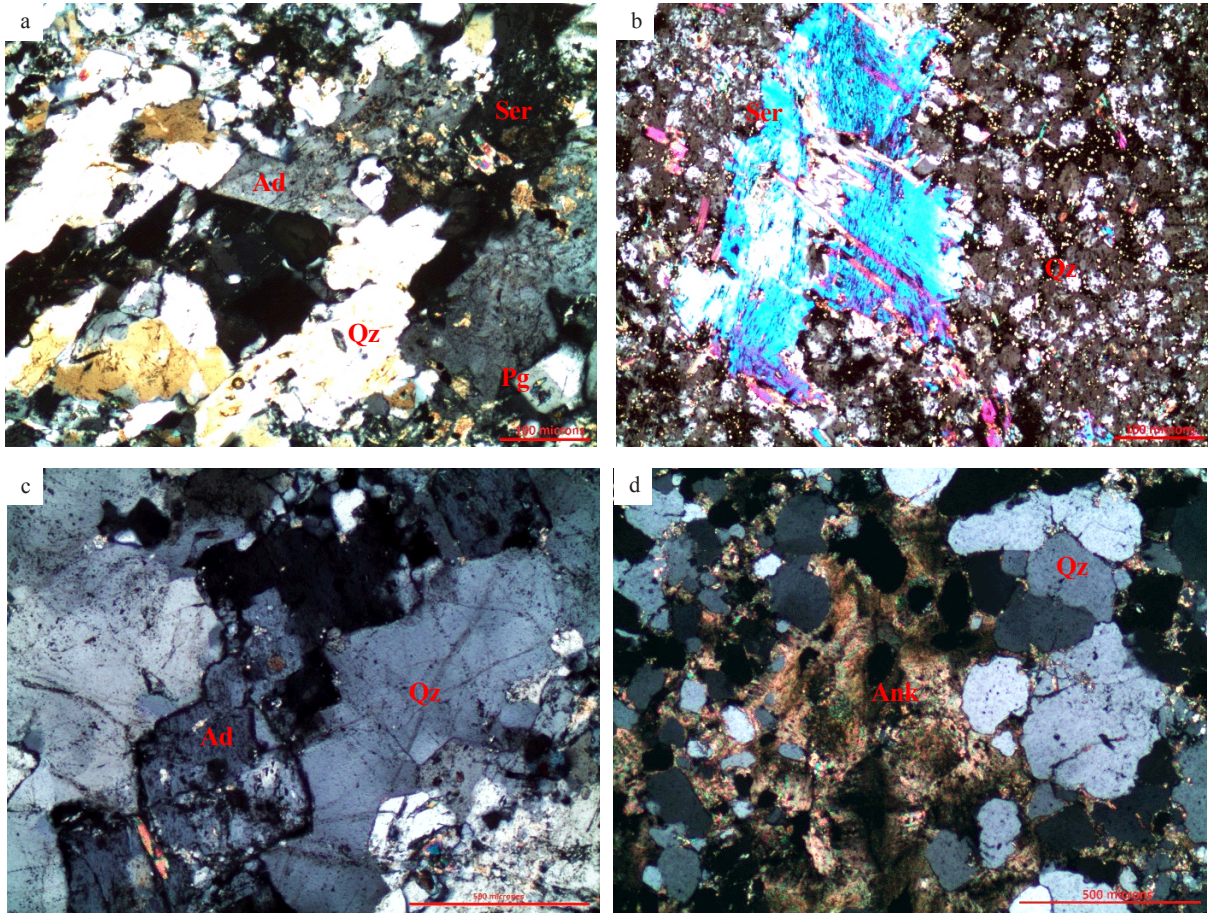


Figure 7. a. Veinlet of adularia in gneiss quartz feldspathic and sericitization on plagioclase, b. Plagioclase with sericitic (coarse sericite) alteration. c. Veinlet of adularia. d. Ankerite and calcite of alteration in quartzmonzonite.

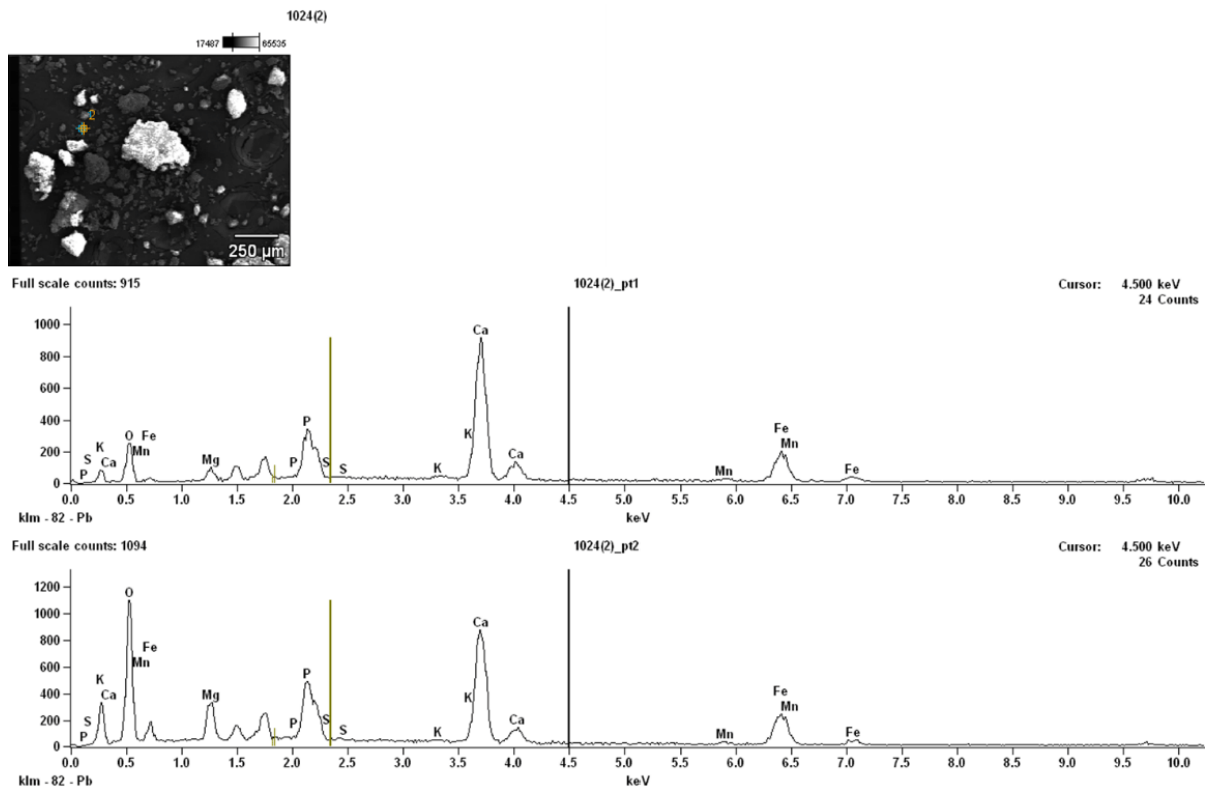
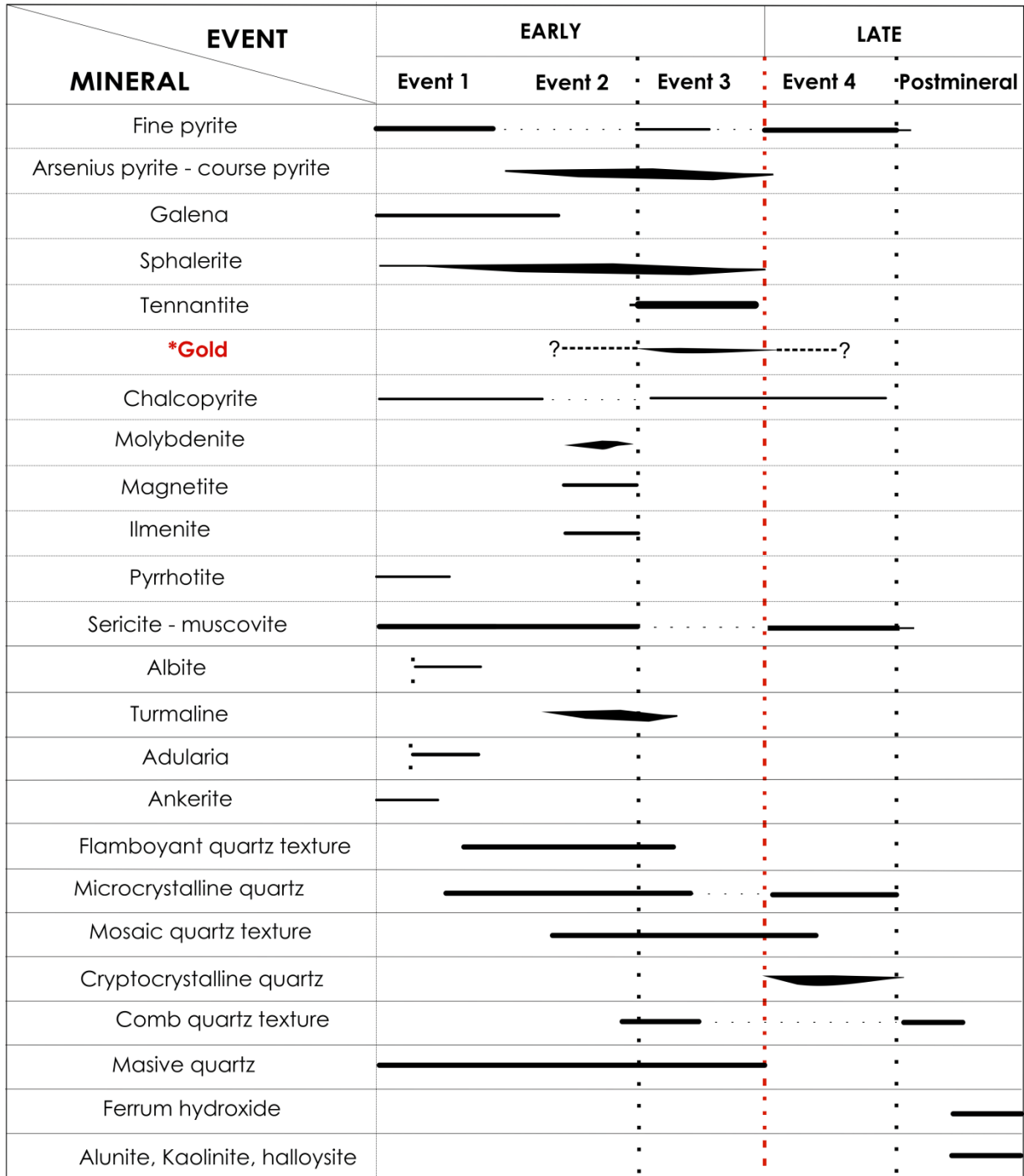


Figure 8. Analysis of ankerite with electronic microscopy was identified calcium, iron and magnesium.

PARAGENETIC SEQUENCE



• • • Fracturing - - - - Brecciation

Figure 9. Paragenetic sequence

Fluid Inclusions that have an evidence of strangulation or fluid leakage was not measured.

Four temperature changes were visualized:

- First Melting Temperature.
- Hydro-halite Melting Temperature.
- Final Melting Temperature of ice.
- Homogenization Temperature.

These temperature changes allowed the authors to not only determine the chemical system but also the minimum trapping temperature, which allowed to determine important variations in temperature during deposit formation.

First melting temperatures are quite low, indicating the presence of salts in the water, and can be divided into three groups of temperature: -40°C to -35°C, -30°C to -25°C and -23°C to -20°C. This range of temperatures show that the composition of the mineralizing fluids was quite complicate, where possibly a saline mixture of NaCl, CaCl₂ and MgCl₂ is presented (table1).

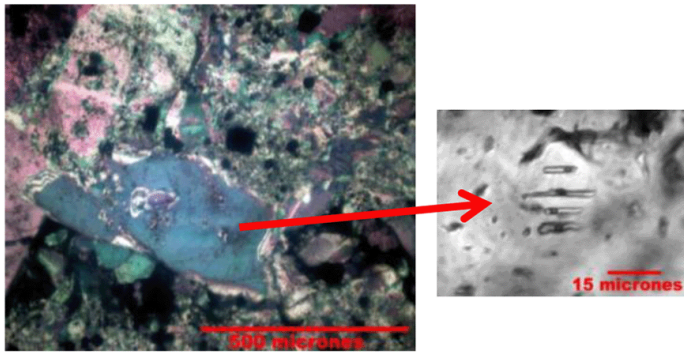


Figure 10. Fluid inclusions in quartz with massive texture of the second mineralizing stage.

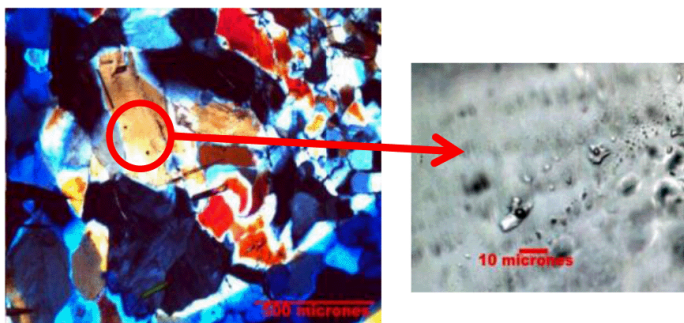


Figure 11. Secondary fluid Inclusions in quartz with flamboyant texture of the third mineralizing event.

In some of the fluid inclusions changes at temperatures between -25°C and -20°C corresponding to the final hydro-halite melting point (table 2). Low temperatures of the first melting and final melting hydro-halite, in most of the measurements in Events 1, 2 and 3 indicate that the chemical system is complex, with at least three different kinds of solutes presented: $\text{H}_2\text{O} - \text{NaCl}$, $\text{H}_2\text{O} - \text{NaCl} - \text{CaCl}_2$, y $\text{H}_2\text{O} - \text{NaCl} - \text{MgCl}_2$, of which NaCl is the predominant, while the MgCl_2 is the lowest in abundance. To determine the presence of these salt systems the following programs were used: AqSo1e, AqSo2e and AqSo3e, Software Package Fluids, Version 1, for aqueous fluid inclusions developed by Ronald Bakker of the University of Leoben in Austria (Table 2).

First melting temperatures are also variable, and generally low, being samples between -6°C to 0°C and others between -12°C to -8°C , that in terms of salt concentration correspond to approximate salinities of 16 wt%eqNaCl to 11 wt%eqNaCl and

10 wt% eqNaCl to 0 wt%eqNaCl respectively. Inclusions related to the early mineralizing events are a little more saline, for example, for the first and second stage the salinity may be above 10 wt%eq NaCl, for the case of second stage can be up 18 wt %eqNaCl (for the first stage 12 wt %eqNaCl), meanwhile for the third and post mineral stage only achieve to 10 %eqNaCl (figure 12).

Fluid inclusions of the first mineralizing stage show that temperatures are between 210°C and 250°C , with an average of 220°C and minimum trapping pressure (calculated using the Software Package Fluids, version 1. of Zhang and Frantz, 1987), varies from 1 to 2 MPa and depths calculated in general under 1000 m, showing that the conditions were propitious for the formation of epithermal deposits (Camprubi & Albinson, 2006).

The second mineralizing stage show a significant increase in the homogenization temperatures, reaching values above 350°C (the range the temperatures is from 227 to 387°C), with an average of 279°C . These high temperatures are consistent with the presence of minerals such as tourmaline, and molybdenite in this event. Values calculated show a minimum pressure range from 3 to 9 Mpa, these being higher values compared to the first mineralizing event. This change in conditions could be explained as an increase in pressure associated with the emplacement of igneous bodies that heated the system contemporaneous with the second mineralizing stage like was observed in the Reina de Oro Tunnel.

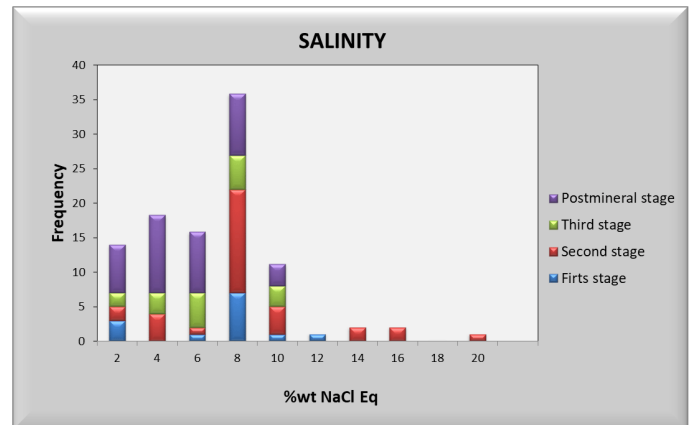


Figure 12. Histogram showing the salinity of fluid for the stage measured. The salinity is similar for the all satage, but for the second event is showing some pikes of salinity, and the most dates are between 6 and 10 %wt NaCl eq.

The fluid inclusions in the third mineralizing event measurements show a decrease in temperature, ranging between 200°C and 240°C , this change is also evident in the mineral assemblages presented in this event, where high-temperature minerals were not identified. The calculated pressures are from 1 to $2,8\text{MPa}$, which are similar to the first mineralizing event.

For the fourth mineralizing event it was not possible to make any microthermometry measurement, because the quartz type present in this event is very fine-grained, cryptocrystalline quartz. However according to the mineralogical scarcity could be inferred that fluids were becoming more impoverished, and the fluid continuous with the cooling process.

In the post-mineral mineralizing event few measurements were made because most inclusions were found liquid-rich, biphasic or with a very small size. Of the few that could be measured, low homogenization temperatures were obtained from 125°C to 190°C (Figure 13).

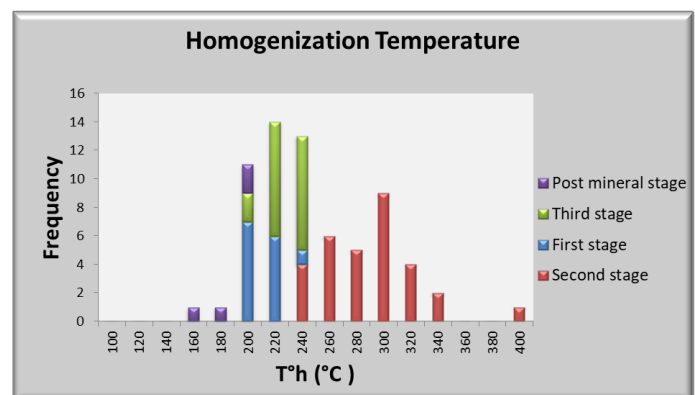


Figure 13. Histogram showing the homogenization Temperature.

Stable isotopes

Around 25 sulfur isotope analysis ($\delta^{34}\text{S}$) in pyrite and galena, 7 isotopes of O ($\delta^{18}\text{O}$) and 6 isotopes H ($\delta^2\text{H}$) were performed.

These analyzes were carried out in the laboratory of the United States Geological Survey USGS for stable isotopes in Denver, Colorado ($\delta^{34}\text{S}$, $\delta^{18}\text{O}$ and $\delta^2\text{H}$) and University of Salamanca in Spain ($\delta^{18}\text{O}$ and $\delta^2\text{H}$). The results of isotopic analysis $\delta^{34}\text{S}$ are reported, based on the standard values of troilite from Diablo's Canyon; for $\delta^2\text{H}$ and $\delta^{18}\text{O}$ isotopes values are given according to the isotopic signature of seawater.

Deuterium and oxygen analyzes were performed into sericite and quartz. Sericite was separated from samples of mineralized veins and backups, which were crumpled and pulverized, and quartz was obtained from mineralized veins.

Table 2. Measurements and calculated parameters from fluid inclusions microthermometry. The analyses of microthermometry was doing with the Bakker – FLUID, software AqSo1e AqSo2e y AqSo3e y Loner 38, for the watery inclusions. (T ff: first fusion, Thh: final fusion of hydrohalite, Tff: Final fusion of ice, Th: homogenization temperature, L: Liquid, V: Vapor).

	No.	Sample	N° Chip	T°ff	T°fhh (°C)	T°ffi (°C)	T°h (°C)	homogenization (L o V)	Salinities %wt NaCl Eq	NaCl %	CaCl ₂ %	MgCl ₂ %	Minimum pressure	Densities (g/cm ³ a 25°C)	Depth (m)
FIRST STAGE	1	1005	(1)-(2)	-29	-22	-12	237,5	L	16	15,6	0,3		2,8	1,13	253
	2	1005	(3)-(1)	-30		-4,5	237,5	L	7,2	3	5		2,8	1,07	267
	3	1005	(3)-(2)	-27,7	-23,9	-4,5	230	L	7,2	6,8	0,6		2,4	1,06	232
	4	1005	(5)-(1)	-32,2	-25,5	-4,3	207	L	7	6,1	1,1		1,5	1,06	142
	5	1005	(15)-(2)	-30,2	-26,1	-1,1	240,7	L	1,9	1,5	0,3		3	1,02	299
	6	1022	(1)-(1)	-30	-23,6	-0,3	220	L		0,4		0,2	2	1	198
	7	1022	(1)-(4)	-30	-21,5	-0,8	220,4	L	1,4	1,2	0		2	1,01	198
	8	1022	(6)-(2)	-30	-21	-4,8	233,1	L	7,6	7,8			2,6	1,06	246
	9	1022	(9)-(1)	-30	-21,9	-8	217,7	L	11,7	11,7	0,2		1,9	1,1	173
	10	1035	(5)-(2)			-1,1	236,7	L	1,9	1,9			2,8	1,21	276
	11	1035	(7)-(2)	-31,8	-24,8	-6,3	202	L	9,6	8,7	1,1		1,3	1,05	124
	12	1035	(13)-(1)	-23,3		-3,8	219	L	6,2	5,6	0,8		1,9	1,05	162
	13	1035	(14)-(2)	-6,7		-3,7	217,7	L	6	6				1,06	
	14	1035	(14)-(1)	-23,7	-22,9	-3,8	209	L	6,2	6,1	0,3		1,9		180
	15	1043	(4)-(1)	-24,9		-4,6	222,9	L	7,3	6,7	0,9		2,1		200
SECOND STAGE	1	1005	(16)-(2)	-42,2		-3,4	274,9	L	5,6	0,6	5,7		5,5	1,01	531
	2	1005	(17)-(1)	-32,4	-23,2	-15	241,1	L	18,6	17,5	1		3	1,15	266
	3	1005	(17)-(2)	-27	-23,2	-3,8	282	L	6,1	6	0,3		6,2	1,05	600
	4	1022	(7)-(1)	-30	-22,6	-4,5	284,1	L	7,2	7,1	0,3		6,4	1,06	616
	5	1022	(8)-(1)	-29,6	-20,8	-1,2	291	L	2	2,1			7,1	1,02	712
	6	1022	(13)-(1)	-30	-22,6	-1,9	292,5	L	3,2	3,1	0,1		7,3	1,03	722
	7	1035	(1)-(1)		-21	-4,3	257,6	L	6,9	6,9			4,1	1,06	395
	8	1035	(13)-(2)		-24,3	-3,8	242	L	6,2	5,8	0,6		3,1	1,05	297
	9	1035	(13)-(3)		-25	-2,2	242	L	3,7	2,4	1,7	0,6	3,1	1,03	303
	10	1035	(11)-(1)	-24,2	-23,9	-0,7	243	L	1,2	1		0,5	3,1	1,01	314
	11	1043	(1)-(6)		-23,5	-3,8	295	L	6,2	5,9	0,4		7,6	1,21	638
	12	1043	(3)-(1)	-25		-10	301,5	L	13,9	12,2	1,7		8,3	1,13	760
	13	1043	(4)-(2)	-22,5		-4,3	309,4	L	6,9	6,9	2,6		9,3	1,07	890
	14	1043	(4)-(3)	-25		-3,5	329	L	5,7	2,2	6,1		12,2	1,06	1170
	15	1043	(10)-(1)	-30	-20,3	-1,8	387,6	L	3,1	3			23,9	1,03	2373
	16	1043	(10)-(4)	-30,1	-21,3	-4,8	280,8	L	7,6	7,6			7,4	1,06	729
	17	1043	(10)-(5)	-28,5		-4,3	237,1	L	6,9	2,6	6,1		2,8	1,07	266
	18	1043	(11)-(1)	-28,2		-5,4	293	L	8,4	8,2	0,3		9,3	1,07	889
	19	1043	(11)-(2)	-29		-5,2	280	L	8,1	2,6	6,1		6	1,08	566
	20	1043	(7)-(2)	-28,9	-24,4	-4,4	232,8	L	7	6,6	0,7		2,6	1,068	246
	21	1043	(8)-(1)	-28,4		-2,4	274,6	L	4	1,5	3,1		5,5	1,04	537
	22	1043	(8)-(2)	-33,5		-12	298	L	16	3	12,7		7,9	1,15	704
	23	1043	(8)-(3)	-30		-12	229	L	16	4,2	11,6		2,4	1,15	210
	24	1014	(2)-(2)	-30	-19	-5	271	L	8	7,9			5,2	1,07	495
	25	1014	(2)-(1)	-29	-20	-4,4	288	L	7	7			6,8	1,06	655
	26	1014	(7)-(2)	-25		-4,6	250	L	7,3	7,3			3,6	1,06	343
	27	1014	(9)-(2)	-30	-22,6	-10	262	L	14	13,5	0,5		4,4	1,12	405
	28	1014	(2)-(4)	-24,6	-20	-5	319	L	8	7,9			10,7	1,07	1019
	29	1014	(8)-(1)	-28	-22,6	-6,4	329	L	9,7	9,6	0,3		12,2	1,08	1146
	30	1014	(2)-(3)	-25,2	-21	-5	303	L	7,9	7,9			8,5	1,07	815
	31	1014	(4)-(4)	-30	-25	-5,3	227	L	8,3	7,5	1,1		2,3	1,07	216
	32	1014	(9)-(1)	-30	-21,7	-5	272	L	7,9	8	0,8		5,3	1,07	503
THIRD STAGE	1	1005	(1)-(1)	-28,5	-25,7	-12	214,5	L	16	13,2	2,6		1,7	1,13	156
	2	1005	(6)-(1)	-30	-23,8	-2,5	207,4	L	4	3		1,5	1,5	1,04	146
	3	1005	(6)-(2)	-30	-23,8	-2,5	207,4	L	4	3		1,5	1,5	1,04	146
	4	1005	(6)-(3)	-35,7		-5,8	227,4	L	8,9	3,4	6,1		2,3	1,04	215
	5	1005	(6)-(4)	-41,2	-21,2	-1	230,4	L	1,7	1,66			2,4	1,02	244
	6	1005	(9)-(1)	-25,2	-20,4	-3	238,4	L	5	5,7	0		2,9	1,04	279
	7	1005	(15)-(1)	-31	-22,5	-4,5	199,8	L	7,2	7,1	0,2		1,3	1,06	121
	8	1005	(15)-(3)	-31	-25,9	-2,6	213,4	L	4,3	3,77	0,8		1,8	1,04	166
	9	1005	(16)-(3)	-30	-20,9	-2,7	222,9	L	4,55	4,55	0		2,1	1,04	204
	10	1022	(10)-(1)	-30	-25,5	-2,5	234	L	4,2	2,5		2,1	2,6	1,04	257
	11	1035	(19)-(1)		-21,9	-2,2	225	L	3,7	3,5		0,4	2,2	1,03	215
	12	1035	(19)-(2)		-22,6	-4	196,5	L	6,4	6,4	0,2	1	1,2	1,06	113
	13	1043	(1)-(3)	-23,5		-6,3	217,1	L	9,66	9,2	0,6		1,8	1,08	174
	14	1043	(1)-(5)	-23,7		-4,6	238	L	7,3	7	0,5		2,8	1,06	272
	15	1043	(2)-(1)	-23,4		-3,8	221	L	6,2	6	0,4		2	1,05	194
	16	1043	(5)-(3)	-20		-4,8	216,5	L	7,6	7,66			1,8	1,06	174
	17	1043	(5)-(1)	-27,9	-24,1	-6,1	217,2	L	9,3	8,6	0,8		1,8	1,08	174
	18	1043	(5)-(2)	-25		-3,3	216,5	L	5,4	4,9	0,7		1,8	1,05	175
	19	1043	(7)-(1)	-26,9		-0,9	214,5	L	1,66	0,9	0,8		1,8	1,02	180
POST MINERAL STAGE	1	1005	(1)-(3)	-32		-0,9	125,4	L	7				0,5	1,1	41
	2	1005	(8)-(1)	-24,6		-7,7	187	L	11,3				0,9	1	93
	3	1005	(18)-(2)			-5,8	169,9	L	8,9				0,7	1	65
	4	1005	(18)-(3)			-5,8	188,6	L	8,9				0,5	1,1	43
	5	1022	(6)-(1)	-23,1		-1,9	142	L	3,2				0,5	1	45

Sulfur isotopes

Isotope values for $\delta^{34}\text{S}$ show a bimodal trend with values between 1 ‰ to -6 ‰ and -17.6 ‰ to -20 ‰ (Figure 14), indicating two different sources of sulfur. The closer to zero values are associated with felsic igneous rocks (Campbell & Larson, 1998), sulfur was possibly leached from the sulfides presented in igneous rocks (Rye & Ohmoto, 1974). The most negative $\delta^{34}\text{S}$ values are the result of leached of metamorphic rocks (from sedimentary) for reactive fluids during hydrothermal process, and imposed their isotopic signature to mineralization (Tang et al., 1998 from Y. Zhang et al., 2017)

Table 3. Isotope ($\delta^{34}\text{S}$ (‰)) results for mineral separates

Sample	Mineral	$\delta^{34}\text{S}$ (‰)
1003	Py	0,48
1009	Gn	0,0
1009	Py	-1,2
1010	Py	-0,44
1012	Py	-5,7
1014A	Py	0,9
1018	Py	-0,6
1019A	Py	-2,0
1022	Py	-3,4
1028	Py	0,7
1031	Py	-16,7
1031	Py	-17,8
1033	Py	1,4
1034	Py	0,8
1035	Py	-3,4
1043	Py	2,5
1019	Py	-0,6
1050	Py	1,0
1050	Ga	-19,0
1050	Ga	-20,0

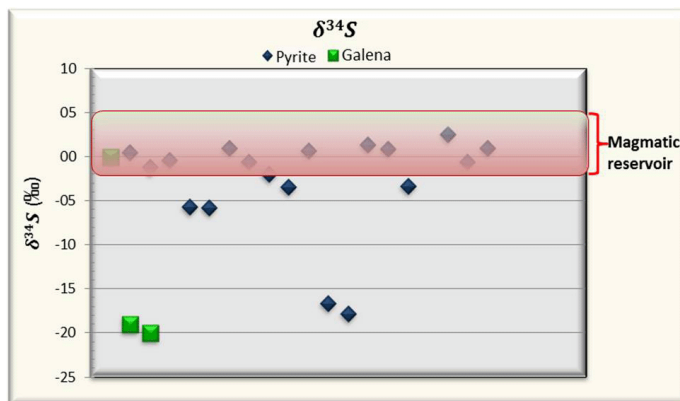


Figure 14. Sulfur isotope analysis ($\delta^{34}\text{S}$)

Deuterium and oxygen isotopes

Analyses were performed on samples obtained from quartz veinlets and sericite from the alteration zone of the host rocks in the vein zone.

The isotopic values of $\delta^{18}\text{O}_{\text{SMOW}\text{‰}}$ are close to 10 indicating that fluid have strong magmatic affinity

(Campbel & Larson, 1998), in the case of $\delta\text{D}_{\text{SMOW}\text{‰}}$ the situation is the same the most values have magmatic signature (Campbel & Larson, 1998).

When deuterium and oxygen results are compared it (Figure 15), a strong magmatic affinity is observed. This affinity is illustrated by the fact that most of the points fall very close to the field of magmatic waters and even two of the values are within the field. The points that are outside of this field tend to move toward the line of meteoric water, indicating that they are also related.

According to the previous facts it can be interpreted that the mineralizing fluids were generated due to a mixture of meteoric and magmatic waters, being magmatic waters dominant.

Table 4. Stable isotopes of deuterium and oxygen results

Muestra	Mineral	$\delta^{18}\text{O}_{\text{SMOW}\text{‰}}$	$\delta\text{D}_{\text{SMOW}\text{‰}}$	Isotopic fractionation factor of O (1000 ln α_{A-B})	H ₂ O%
1002	Sericite	11,2	-77,1	5,95	2,3
1014	Quartz	11,4	-	4,86	0,3
1018	Quartz	15,7	-77,6	9,16	0,3
1022	Quartz	11,8	-88	2,08	0,3
1035	Quartz	13,2	-80,7	3,40	0,5
1035	Quartz	13,1	-80,7	3,30	0,5
1043	Quartz	13,6	-93,8	5,23	0,4
1035	Sericite	12,9	-	8,50	--

When deuterium and oxygen results are compared it (Figure 15), a strong magmatic affinity is observed. This affinity is illustrated by the fact that most of the points fall very close to the field of magmatic waters and even two of the values fall within the field. The points that are outside of this field tend to move toward the line of meteoric water, indicating that they are also related.

According to the previous facts it can be interpreted that the mineralizing fluids were generated due to a mixture of meteoric and magmatic waters, being magmatic waters dominant.

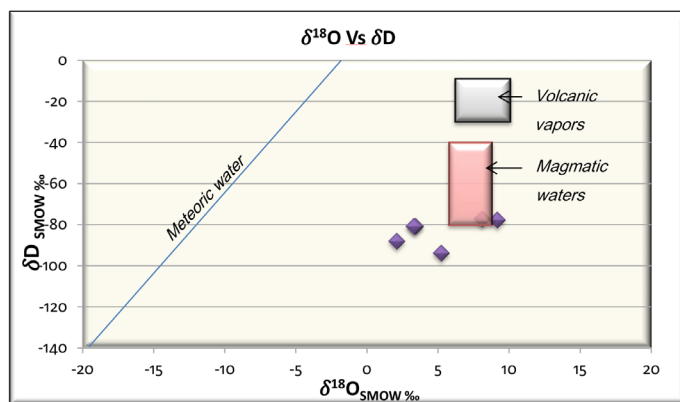


Figure 15. Diagram of $\delta^{18}\text{O}$ vs δD . Modified from Taylor, 1979 in Barnes, 1997

Ore deposit age

Four rock samples were taken from three different veinlets; these were chosen according with their high content of sericite.

The rock samples were pulverized, sieved and clays were separated by decanting. In the case of thicker sericite these were separated by *hand picking* method under stereomicroscope. The samples were analyzed in the laboratories of the University of Oregon.

As shown in the Table 5 and figure 16, mineralization originated from Miocene to Pliocene, where 3 different hydrothermal pulses were identified, the oldest at 10.78±0.23 Ma, an intermediate between 7.68±0.15 Ma and 6.89±0.41 Ma and the last one of 5.24±0.10Ma. The first pulse could be contemporaneous with intrusion bodies, one of them a granodiorite with age is (U/Pb on zircon) 10.9±0.2 Ma, located in the Meseton sector (Mantilla et al, 2011) 1 to 3 Km at NW of mineralizations visited on Vetás, indicating that body like that could be source of fluids and temperature for the first stage of the mineralization.

The others ages 7.68±0.15Ma and 6.89±0.41Ma could be with the second and possibly third stage, because the petrography in that samples corresponding with that stages, and the 5.24±0.10Ma corresponding to fourth stage.

Also, there are some intrusive rhyodacitic bodies younger in the area with age from 8.4±0.2 y 9.0±0.2 Ma (Mantilla et al, 2009), that indicate that the magmatism was continue for a long time, and contribute to warm and elements to mineralizing fluids. It's therefore possible there are intrusive bodies younger no date in the area

Table 5. Ar/Ar age of the analyzed samples

AGES OBTAINED FOR MINERALIZATIONS				
Sample number	Mineral for analyzing	Rock type	Age plateau (My)	Age inverse isochron (My)
1002	Sericite	Vein (Loscas North)	10.78 ±0.23	11.53±0.84
1012	Sericite	Backup Vein, La Gloria mine	5.24 ±0.10	5.26±0.13
1018	Sericita	Backup vein, Salvación mine	7.68±17	6.75±0.1
1018D	Sericite	Backup vein, Salvación mine	7.58 ±0.15	7.19±0.54
1022	Sericite	Vein, La Locura mine	6.89 ±0.41	6.83±059

Discussion

The Vetás gold deposit was formed by four mineralizing events and one post-mineral event. The first stage shows typical neutral characteristics of low sulfidation epithermal environments according to their mineralogical association, fluids composition, low saline and temperature of deposit formation (Camprubi et al., 2003). For the second event, conditions change, due to temperature increase associated with the possible injection of hot and mineral-rich fluids to the system, increasing salinity slightly in fluids. During the second stage, the magmatic influence is more evident than the first stage, such as the stable isotopes with a magmatic signature, seems greater relationship with marginal porphyritic conditions, overlap intermediate epithermal environment on the initial conditions.

The fluid which interacted with the host rocks, was cooled, developed, neutralized and mixed with meteoric water, precipitating minerals with intermediate sulfidation like sulfosalts (tennantite) silver-rich and zinc-rich, plus gold, low iron sphalerite, pyrite and chalcopyrite (Yilmaz, et al., 2010; Wang et al, 2019). In the third mineralizing event, fluid and had lower salinity.

Possibly due to an increase in pressure, a hydraulic micro-brecciation, whose matrix is composed of cryptocrystalline quartz and pyrite is generated. The little mineralogy could be showing that the fluid was getting colder and low in dissolved elements when the four stage happened.

Finally single crystals of quartz with “comb” texture were precipitated in the open spaces, at temperatures below 190°C.

Such magmatic influence on the ore deposit becomes more apparent during the second hydrothermal event where a drastic increase in temperature (>300°C) found by measurement of fluid inclusions and represented by the mineralogy presented during this event is observed. This mineralogy is characterized by high-temperature minerals such as molybdenite, magnetite and tourmaline, showing almost porphyritic features, possibly caused for the overprinted of different hydrothermal systems, product of continue magmatism for 2.5 Ma during Mioceno (Mantilla et al., 2011), the first one, previous to

contemporaneous with the first hydrothermal stage with of 10, 9± 0.2 Ma (U / Pb zircon, Mantilla, et al 2011), and the other one dated with 8.4 ±0.2 y 9.0 ± 0.2 Ma (Mantilla et al, 2009), before second stage (7,58±0,15Ma and 6,89±0,41Ma), but is necessary dated others porphyritic bodies identified in the area to check their real relation with different stages of the mineralization, being that the magmatic affinity is important.

The mineralogical association and salinity of the mineralizing fluids, strong magmatic affinity evidenced with isotopic results, in addition to the pressure and temperature conditions allow the classification of the ore deposit as intermediate sulfidation epithermal deposit (Hedenquist et al, 2000, Camprubi & Abilson, 2006, Yilmaz, et al., 2010 and Wang et al, 2019). Those characteristic could be originated for entry of fluids magmatic and warm to the system during the second stage, that magmatic influence could be over print marginal porphyritic conditions, but is necessary check cores to verify the presence porphyry on depth.

Solutions neuters to alkaline (illite –sericite association) and low salinity at temperatures near 330°C, allow the conclusion that gold could be transported by bi- sulphides complexes to shallow levels where the ambient is most oxidant and possibly most acid allowed more precipitation. (Hedenquist et al. 2000, Camprubi et al. 2006, Williams-Jones, et al., 2009).

Metallogenic model

The low to intermediate sulfidation epithermal ore deposit located in Vetás, Santander, originated in a tectonic framework associated with The Bucaramanga fault (main structure) and crossings structures with strikes of NE and NW, which helped as a duct for the magmas ascending, product of Caribbean Plate depth subduction under the South American Plate (Mantilla et al. 2011) .

These magmas with ryodacitic to quartz-monzonites composition were important in the ore deposit formation; because they were initially the main source of mineralizing fluids. The first one of 10, 9± 0.2 Ma (Mantilla et al, 2011), was the source of first stage possibly, and 8.4 ±0.2 and 9.0 ± 0.2 Ma (Mantilla et al, 2009) of second stage, even though other bodies more recent no dated.

Between the Miocene - Pliocene, magmatic fluids, reacted with Bucaramanga gneiss rocks and intrusive igneous rocks (Jurassic and Tertiary) altering it. During the first stage (10.78 ±0.23) these fluids were mixed with meteoric water; they were neutralized and the metals were transported by bi-sulphides complexes because according with the alteration mineralogy (illite – sericite - carbonates), and temperature (200 to 240°C in the first stage) was the most appropriated mechanism, on shallower depth the enviroments is most oxidant and the metals deposited on open spaces in an low sulfidation environment.

A magmatic pulse between first and second stage of 8.4 ±0.2 and 9.0 ± 0.2 Ma was identified to 8 km NW approx. this pulse could be related to the second stage (7,58±0,15Ma and 6,89±0,41Ma). The difference between ages is almost 1 Ma, but is possible the presence of others bodies no dated but identified in the area (Figure 1). The mechanism of transported to the second stage its considered similar to the first stage, but the mineralogy, the fluid inclusions show more temperature and stable isotopes more magmatic affinity, this aspects allow suggest that overprinted a system of intermediate sulfidation to almost marginal porphyritic conditions on low sulfidation environment.

The third stage is considered like a progression of second stage, but with the coolest and poorest (in metals) fluid, was separated of first event because the minerals were deposited in new spaces opened, product of fracturing event. The four stage dated with (5.24 ±0.10 Ma), could be representing a progression on the fluid evolution, with more interaction of meteoric fluids, produce a hydraulic brecciating (Mciver, 1997). The post mineral stage is the continuation of evolution of fluid colder and poor in metals, possibly on areas close to surface with a strong oxidation activity and an acid ph (alunite, kaolinite and halloysite).

Conclusions

- Vetás gold deposit, Santander, is a low to intermediate sulfidation epithermal ore deposit in which this study has identified four mineralizing events and one post-mineral event.

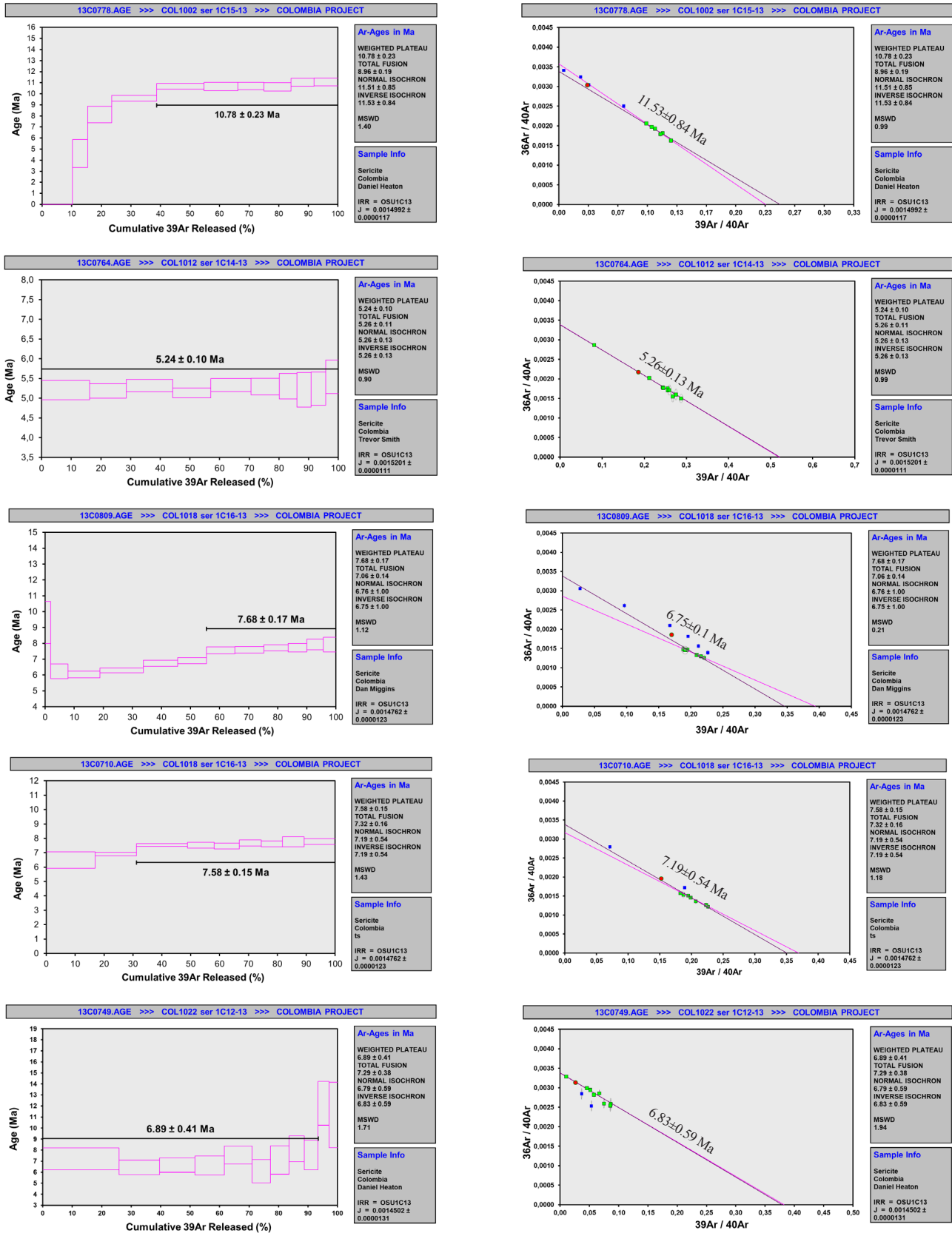


Figure 16. Age plateau and inverse isochron. The graphics show satisfactory results because the plateaus are almost perfect, with exception to the samples 1002 and 1018 (duplicate), where the 10% of the released gas is below the average age and the sample and the sample 1022 where 10% of the last released gas is above of the average age. The ages calculate with the inverse isochron are very similar to the plateau values, even though in some case there are small variations but those values are into the margin of error, only in the case of sample 1018 the values are more scattered, for this reason the assay was repeated.

- Fluids salinity is high and complicated because there are at least three types of chemical systems: NaCl- H₂O, CaCl₂ - NaCl - H₂O y MgCl₂, - NaCl - H₂O, with concentrations reaching up to 16% wteqNaCl for the first and third mineralizing events, 18 % wteqNaCl for the second event and 8 to 10% wteqNaCl for the post-mineral event. These values of salinity are similar of low and intermediate epithermal gold deposits in Mexico (Camprubi & Albinson, 2006).
- The Ore deposit was formed from Miocene to Pliocene (between 10,7Ma - 5,6 Ma), this time period is contemporaneous during the first 2.5 Ma with magmatic bodies dated on the area by Mantilla et al, (2009; 2011). This magmatism had a strong relationship with the actual configuration of deposit, evidenced on stable isotopes result and the temperature pikes (second stage mainly). Then this magmatism could overprinted marginal porphyritic features to the deposit in the second stage, evidenced on the temperature (390°C), high temperature mineralogy, and caused environments with intermediate sulfidation characteristics.
- Stable isotopes of δ¹⁸O, δ²H, allow to infer that the mineralizing fluids were a mixture of meteoric and magmatic waters where the latter are dominant.
- Stable isotopes of δ³⁴S, show a magmatic reservoir to the mineralization principally, and other possible reservoir is from sedimentary metamorphic rocks of Bucaramanga Neis, one of the host rocks in the area.
- The alteration minerals like Sericite, carbonates and illite shows that mineralizing fluids were neutral, except on the postmineral stage that be shallower and environment more oxidant the pH was more acid (alunite, kaolinite and halloysite).
- The identified gold is associated to tennantite and low-iron sphalerite, this was possibly carried by bi- sulphides complexes, according to neutral pH, homogenization temperature and the ore deposit formation depth.
- Although free phase silver not was identified, this chemical element is part of the tennantite composition, where it is found in high proportions.

RECOMMENDATIONS

- Make a petrographic, geochemical and geochronology study of the intrusive bodies outcropping in the NE of Vetas town, in order to differentiate accurately Miocene (Pliocene?) igneous pulses there, clearly determine their chemical characteristics and their associated tectonic environment.
- Date directly the metallic mineralization with methods like Re/Os in molybdenite.
- Produce a hydrothermal alteration map and make a review of drilling hunches in order to establish their possible association with porphyry ore deposit.

Acknowledgments

The authors would like to thank The United States Geological Survey (USGC), Universidad Nacional de Colombia and the IGAC Geographic Institute for their collaboration in the development of analytical process. In addition, the authors are very grateful to the CB Gold Company for logistical support and all artisanal miners who allowed us to work on their projects and be in their tunnels.

References

- Barnes, H. L. I. (1979). *Geochemistry of hydrothermal ore deposits*. I. Wiley & Sons. 797 - 804 p.
- Bakker, R. J. (2003). Package FLUIDS 1. Computer programs for analysis of fluid inclusion data and for modeling bulk fluid properties. *Chemical Geology*, 194, 3-23.
- Camprubi, A., González, E., Levresse, G., Tritilla, J. & Carrillo, A. (2003). Depósitos epitermales de alta y baja sulfuración: una tabla comparativa. *Boletín de la Sociedad Geológica Mexicana*, Tomo LVI, No. 1, 10-18.
- Camprubi, A. & Albinson, T. (2006). Depósitos epitermales en México: actualización de su conocimiento y reclasificación empírica. *Boletín de La Sociedad Geológica Mexicana, volumen conmemorativo del centenario*, Tomo LVIII, 1, 27-81.
- Campbell, A. R. & Larson, P. B. (1998). Introduction to stable applications in hydrothermal systems. *Reviews in Economic Geology*, 10, 173-192.
- Cortés, Y. (2002). *Caracterización metalográfica aplicada a la optimización de los procesos de recuperación de oro en la Mina Reina de Oro, Veta - California (Santander)*. Universidad Nacional de Colombia. Trabajo de grado.
- Demoustier, P. A., Castroviejo, R., & Charlet, J. M. (1998). Clasificación textural del cuarzo epitermal (Au-Ag) de relleno filoniano del área volcánica de Cabo de Gata, Almería. *Boletín Geológico y Minero*, 109, 449-468.
- Dong, G., Morrison, G. & Jaireth, S. (1995). Quartz textures in epithermal veins, Queensland; classification, origin and implication. *Economic Geology*, 90, 1841-1856.
- García, C. & Uribe, E. (2003). Los Delirios: un yacimiento hidrotermal de oro y plata en la región de Vetas, Santander (Colombia). Colombia, *Boletín de Geología - Bucaramanga*, 25 fasc. 40, 91-103.
- Hedenquist, W., Arribas, R. A., & Gonzalez-Urien, E. (2000). Exploration for Epithermal Gold Deposits. *SEG Reviews*, 15, chapter 7, 245-277.
- Mantilla, W. & Mogollón, J. (1991). *Evaluación geológica y determinación de las reservas de oro y plata de la mina "La Botella". Municipio de Vetas, Santander*. Universidad Industrial de Santander. Proyecto de grado.
- Mantilla, L. C., Valencia, V., Barra, F., Pinto, J., & Colegial, J. (2009). Geocronología U-Pb de los cuerpos porfíricos del distrito aurífero de Vetas-California (Dpto. de Santander, Colombia). *Boletín de Geología*, 31, 1, 31-43.
- Mantilla, L. C., Mendoza, H., Bissig, T & Craig, H. (2011). Nuevas evidencias sobre el magmatismo miocénico en el Distrito Minero de Vetas - California (Macizo de Santander, Cordillera Oriental de Colombia). *Boletín de Geología*, 33, 1, 43-58.
- Mciver, D. A. (1997). *Epithermal precious metal deposits: physicochemical constraints, classification characteristics, and exploration guidelines Rhode University*. Master Tesis. 141 pags.
- Rojas, S. (2013). *Metageniadelas mineralizaciones auríferas en la zona de Vetas, Santander*. Universidad Nacional de Colombia. Tesis de Maestría. 143 pags.
- Rye, R. O. & Ohmoto, H. (1974). Sulfur and carbon isotopes and ore genesis: A review. *Economic Geology*, 69, 826-842.
- Urueña, C. L. (2014). *Metamorfismo, exhumación y termocronología del Neis de Bucaramanga. (Macizo de Santander, Colombia)*. Universidad Nacional de Colombia. Tesis de Maestría.
- Urueña, C. L. & Zuluaga, C. A. (2011). Petrografía del Neis de Bucaramanga en cercanías a Cepitá, Berlín y Vetas - Santander. *Geología Colombiana*, 36(1), 37-55.
- Wang, L., Quin K., Song, G. & Li, G. (2019). A review of intermediate sulfidation epithermal deposits and subclassification. *Ore Geology Reviews*, 107, 434-456.
- Ward, D., Goldsmith, R., Jimeno, A., Cruz, J., Restrepo, H. & Gomez, E. (1973). Geología de los cuadrángulos H12 Bucaramanga y H13 Pamplona, Departamentos de Santander y Norte de Santander. U.S. Geological Survey, Ingeominas. *Boletín Geológico*, XXI, 1-3, 1p.
- Williams-Jones, A., Bowell, R. & Migdisov, A. (2009). Gold in Solution. *Elements*, 5, 281-287.
- Yilmaz, H., Oyman, T., Sonmez, N., Arehart, G., & Billor, Z. (2010). Intermediate sulfidation epithermal gold-base metal deposits in Tertiary subaerial volcanic rocks, Sahinli/Tespil Dere (Lapseki/Western Turkey). *Ore Geology Reviews*, 37, 3-4, 236-258.
- Zhang, Y. G. & Frantz, J. D. (1987). Determination of the homogenization temperatures and densities of supercritical fluids in the system NaCl-KCl-CaCl₂-H₂O using synthetic fluid inclusions. *Chemical Geology*, 64, 335-350.
- Zhang, Y., Shao, Y., Chen, H., Liu, Z. & Li, D. (2017). A hydrothermal origin for the large Xinqiao Cu-S-Fe deposit, Eastern China: Evidence from sulfide geochemistry and sulfur isotopes. *Ore Geology Reviews*, 88, 534-549.